Energy Advances

ROYAL SOCIETY OF CHEMISTRY

PAPER

View Article Online
View Journal | View Issue

Check for updates

Cite this: *Energy Adv.*, 2025, 4, 1455

Performance enhancement of inverted perovskite solar cells through lithium-ion diffusion from the nickel oxide hole transport layer to the perovskite absorber

Pravakar P. Rajbhandari,[ab] Bipin Rijal,[ab] Zeying Chen,[ac] Ankit Choudhary,[d] Haralabos Efstathiadis[d] and Tara P. Dhakal *[abc]

Received 15th March 2025,
Accepted 2nd September 2025

DOI: 10.1039/d5ya00072f

rsc.li/energy-advances

Inverted perovskite solar cells, known for their low temperature processability and reduced hysteresis, benefit from the use of nickel oxide (NiO_x) as a hole transport material, which enhances stability. The doping of NiO_x with lithium improves its electrical properties by creating Ni^{3+} sites through intrinsic doping with Ni vacancies. This study investigated the impact of Li doping on the optical and electrical properties of NiO_x and evaluated the optimal doping concentration for solar cell performance. Additionally, the diffusion of small sized Li-ions from the NiO_x hole transport layer into the photoactive perovskite layer was investigated, which led to an improvement of the perovskite absorber quality through defect passivation caused by lithium diffusion from the NiO_x layer, enhancing device performance. The incorporation of lithium significantly boosted all solar cell parameters, leading to a 60.8% increase in power conversion efficiency (PCE), from approximately 12% to a maximum of 19.3%.

Open Access Article. Published on 05 September 2025. Downloaded on 6/8/2026 3:32:19 PM.
This article is licensed under a Creative Commons Attribution-NonCommercial 3.0 Unported Licence.

Introduction

Perovskite based solar cells have witnessed tremendous growth in a short period of time and efforts for their commercialization have been the top priority.[1–3] Even though conventional n–i–p (negative–intrinsic–positive) structured perovskite solar cells (PSCs) have achieved the highest performance thus far, there is growing interest in inverted (p–i–n) planar device architecture due mainly to its relatively simple fabrication process and negligible hysteresis effect.[4–6] The basic p–i–n architecture consists of an intrinsic absorber sandwiched between the hole and electron transport layers (HTL and ETL). A wide range of HTLs, both organic and inorganic, have been studied to determine their suitability for use in inverted architecture solar cells. One of the most critical properties of the HTL in inverted structure devices is that its bandgap must be wide enough to allow more light to reach the perovskite absorber layer. Second, the HTL should effectively block electrons from moving toward the front transparent electrode such as indium tin oxide (ITO). Inorganic materials such as nickel oxide (NiO_x) are of particular interest due to their low cost, higher carrier mobility, and chemical stability.[7,8] These inorganic HTLs are not only stable in the presence of the ITO layer beneath them but are also not affected by the following synthesis processes.[9] The cubic p-type semiconductor NiO_x is one of the most promising materials for HTLs in perovskite solar cells, which has several advantages over the other counterparts, such as high transmittance in the visible spectral range and good tolerance to chemical and thermal treatments.[7,10–13] Beyond that, NiO_x has a good band alignment with most of the perovskite absorbers due to its wide band gap (3.5–4.0 eV) and high work function.[6,14,15]

However, the poor conductivity (2.67×10^{-6} S cm^{-1}) of NiO_x limits the hole extraction efficiency, resulting in a high series resistance, which adversely affects the current density (J_{SC}) and fill factor (FF) of the perovskite solar cells.[8] Moreover, the low conductivity also causes hole accumulation at the interface with the perovskite, which leads to increased interfacial recombination and reduced charge transport.[13] The stoichiometric NiO_x ($x = 1$) with a Ni^{2+} oxidation state insulates the charge carriers. The commonly observed p-type conductivity in undoped NiO_x is due to the presence of Ni^{2+} vacancies. However, the ionization energy of Ni^{2+} vacancies is significant, which limits the hole density and conductivity of p-type NiO_x.[8,16] The conductivity of NiO_x can be considerably improved by increasing the concentration of Ni^{3+} ions by introducing nickel vacancies and interstitial oxygen atoms in

[a] *Center for Autonomous Solar Power (CASP), Binghamton University, Binghamton, NY 13902, USA. E-mail: tdhakal@binghamton.edu*
[b] *Department of Electrical and Computer Engineering, Binghamton University, Binghamton, NY 13902, USA*
[c] *Materials Science and Engineering Program, Binghamton University, Binghamton, NY 13902, USA*
[d] *Department of Nanoscale Science & Engineering, University at Albany, State University of New York, Albany, NY 12222, USA*

© 2025 The Author(s). Published by the Royal Society of Chemistry

Open Access Article. Published on 05 September 2025. Downloaded on 6/8/2026 3:32:19 PM.
This article is licensed under a Creative Commons Attribution-NonCommercial 3.0 Unported Licence.

NiO_x crystals.[15] Depending on the fabrication process, the stoichiometry and the corresponding conductivity can be changed. Doping with extrinsic elements with shallower acceptor levels has been the most effective method to enhance the conductivity and adjust the work function as well as band alignment of NiO_x with the perovskite to minimize losses.[8] A deeper work function with a Fermi level around the midgap can enhance the open-circuit voltage (V_{OC}) of solar cells.

A variety of dopants have been investigated to improve the conductivity of NiO_x including Li^+,[7] Cs^+,[17] La^{3+},[18] Cu^{2+},[19] Zn^{2+},[20] Al^{3+},[21] Co^{2+},[22] Ce^{4+},[8] self-dopant Ni^{3+},[23] molecular dopant 2,2′-(per-fluoronaphthalene-2,6-diylidene) dimalononitrile (F6TCNNQ),[24] and co-dopants, such as Li^+:Cu^{2+},[13] Li^+:Mg^{2+},[25] Ce:Zn^{2+}.[26] Monovalent alkali metal lithium (Li) can effectively p-type dope NiO_x, which improves the electrical conductivity without significantly affecting the light-transmitting performance of NiO_x films. Li^+ (Li-ion) (0.72–0.76 Å) has a similar ionic radius to Ni^{2+} (0.69–0.74 Å), which minimizes the doping mismatch and enhances the lattice stability as well.[14] Various techniques, such as spin coating,[27] spray pyrolysis,[9,28] pulsed laser deposition (PLD),[29] sputtering,[30,31] *etc.*, have been used to fabricate Li-doped NiO_x. Li has a relatively shallower acceptor level in NiO_x for Ni-poor/O-rich conditions.[7] The doping is achieved through Ni^{2+} substitutional replacement with Li-ions, which leads to an increase in Ni^{3+} density and improves the electrical conductivity of NiO_x thin films.[32] Doping NiO_x with Li lowers the ionization energy of the Ni vacancies and thus improves the hole conductivity in NiO_x films. The resistivity of NiO_x has been reported to be in the range of 10–10^6 Ω cm.[33] A dramatic decrease in resistivity, down to 0.15 Ω cm, was achieved by increasing Li-ion concentration up to 7% because Li-ions occupy Ni^{2+} substitutional sites, which in turn increases hole density and enhances p-type conductivity.[34] Li-doped NiO_x was also observed to dramatically suppress trap-assisted recombination at interfacial contact compared with PEDOT:PSS due to the improved crystallinity of the perovskite grown on Li-doped NiO_x and the superior perovskite/NiO_x interface.[35] Zhao *et al.* reported the use of Li:NiO/NiO bilayers to improve carrier extraction, transport, and radiative recombination at the NiO/perovskite interface. It was demonstrated that by tuning Li doping amount, the Ni^{3+} ratio in NiO_x films and interfacial oxidation could be controlled, which resulted in improved photovoltaic performance through the incorporation of $Ni^{3+} \leftrightarrow Ni^{2+}$ ion pairs as interfacial passivation species.[14] While the incorporation of alkali metal cations as additives to the perovskite layer has led to a significant reduction in the defect density of the perovskite, the migration of Li-ions from the hole transport layer to the perovskite absorber layer has also been reported to suppress defect formation and hysteresis, thereby enhancing the performance of perovskite solar cells.[36] The migrated Li-ions that reside at the grain boundaries of perovskite crystals were found to attract the photogenerated electrons and repel the holes, which reduced the probability of recombination at those grain boundaries.[37]

Motivated by the above studies, we examined the doping of nickel oxide with Li and demonstrated its impact on the electrical and optical properties of the material. NiO_x was doped with various amounts of Li, which was then used as the HTL in the fabrication of PSCs. The inclusion of Li-ions in the NiO_x HTL in our inverted perovskite solar cell configuration served a dual purpose: firstly, it enhanced the conductivity of NiO_x by making it more p-type; and secondly, the diffusion of Li-ions to the perovskite absorber layer passivated the defect states, which reduced the non-radiative recombination. Although the migration of Li-ions from the charge transport layer to the subsequent perovskite layer has been reported for regular (nip) structured PSCs, this is the first time we have observed such phenomena in inverted (pin) structured PSCs. This led to a significant improvement in the power conversion efficiencies of our solar cells from 12% to more than 19% upon optimal (8% concentration) Li doping, which originated from the significant improvements of short-circuit photocurrent (J_{sc}) and fill factor (FF). This work confirmed that Li-doped NiO_x is a promising hole transport material (HTM) for high-performance inverted PSCs.

Experimental

Materials and methods

ITO-coated plain glass substrates were cleaned by sonicating in acetone and isopropyl alcohol. Subsequently, the substrates were subjected to UV-ozone treatment for 15 min. The fabrication of the NiO_x film was achieved by spin-coating 0.5 M nickel nitrate hexahydrate (Sigma-Aldrich, ≥97%) and ethylenediamine (Alfa Aesar, 99%) in ethylene glycol (Fisher, 99%) on ITO substrates. The doped NiO_x was composed of a controlled percentage of lithium nitrate (Alfa Aesar, 99%) in a 0.5 M solution. The spin-coated films were annealed at 300 °C in air for 1 h. After annealing, the NiO_x-coated substrates were transferred to a glovebox for further processing. A cesium containing triple cation perovskite ($CsFAMAPb(IBrCl)_3$) was fabricated *via* a two-step spin-coating process. Further details on perovskite synthesis can be found in our previous study.[38] Then, the perovskite films were annealed at 140 °C for 20 min. After cooling down, 17 mg ml^{-1} [6,6]-phenyl C_{61} butyric acid methyl ester (PCBM, Nano-C) in chlorobenzene (Sigma-Aldrich, 99%) was spin-coated at 2000 rpm for 40 s and post-baked at 70 °C for 2 min. An additional buffer layer of ZnO (5 nm) was deposited using atomic layer deposition (ALD) at 100 °C. More details on the ALD process can be found in our previous report.[39] The samples were then transferred to the thermal evaporator outside the glovebox to deposit 100 nm of silver.

Characterization

The structural characterization of the perovskite was performed using X-ray diffraction (XRD) on a PANalytical X'Pert PRO X-ray diffraction system, which employed CuKα X-rays and line-focus optics. A Carl Zeiss Supra 55 VP high-resolution scanning electron microscope (HR-SEM) was used to study the morphology of the films. The photoluminescence (PL) was measured using a Horiba PL measurement system with a 532 nm laser and a photomultiplier tube (PMT) detector. Transmittance was measured using an Ångstrom Sun Technologies TF Probe

© 2025 The Author(s). Published by the Royal Society of Chemistry

Open Access Article. Published on 05 September 2025. Downloaded on 6/8/2026 3:32:19 PM. This article is licensed under a Creative Commons Attribution-NonCommercial 3.0 Unported Licence.

UV/Vis spectrophotometer. Time of flight secondary ion mass spectroscopy (TOF-SIMS) analysis was carried out using an IONTOF Time of Flight SIMS (TOF-SIMS) spectrometer. Details on the experimental procedure of TOF-SIMS measurement can be found in the supplementary information (SI) file. *IV* measurements were carried out using a Keithley 4200-SCS semiconductor characterization system along with a solar simulator from Photo Emission Tech. Cells were tested under AM1.5G 100 mW cm^{-2} illumination with the voltage swept in the forward and/or reverse directions with a scan rate of 0.4 V s^{-1}. External quantum efficiency (EQE) measurement was performed using an EQE system from PV Measurements, Inc. The XPS study was performed using a Surface Science Instruments SSX-100 with an operating pressure of $\sim 2 \times 10^{-9}$ Torr. Monochromatic Al Kα X-rays (1486.6 eV) with 1 mm diameter beam size were used. Photoelectrons were collected at a 55° emission angle. A hemispherical analyzer was used to determine electron kinetic energy using a pass energy of 150 V for wide/survey scans and 50 V for high-resolution scans. A flood gun was used for charge neutralization of non-conductive samples. The band structure of the film was measured using ultraviolet photoelectron spectroscopy (UPS) with He–I as the excitation source. The UPS samples were prepared on ITO substrates.

Results and discussion

Study of the NiO_x hole transport layer

The deposition of the undoped NiO_x film was first optimized. We initially determined the optimal annealing temperature for the NiO_x layer to be 300 °C by comparing the optical transmission of NiO_x films annealed at various temperatures (Fig. S1). Subsequently, the thickness of the NiO_x film was controlled by adjusting the concentration of the precursor solution, which consisted of nickel nitrate hexahydrate and ethylenediamine dissolved in ethylene glycol, and the spin speed. To further investigate the impact of HTL thickness on device performance, we fabricated complete solar cell devices incorporating NiO_x layers with varying thicknesses. The device configuration is shown in Fig. 1(a), where the perovskite layer is deposited using a two-step spin-coating method, following the optimized procedures described in our previous study.[38] The obtained NiO_x film thicknesses and the corresponding device performances are presented in the SI (Fig. S2–S4). Based on this experiment, an optimal and reproducible NiO_x film thickness of about 25 nm was achieved with a precursor concentration of 0.5 M and a spin speed of 5500 rpm.

We then employed the optimized fabrication approach described above to investigate the effect of Li doping on NiO_x.

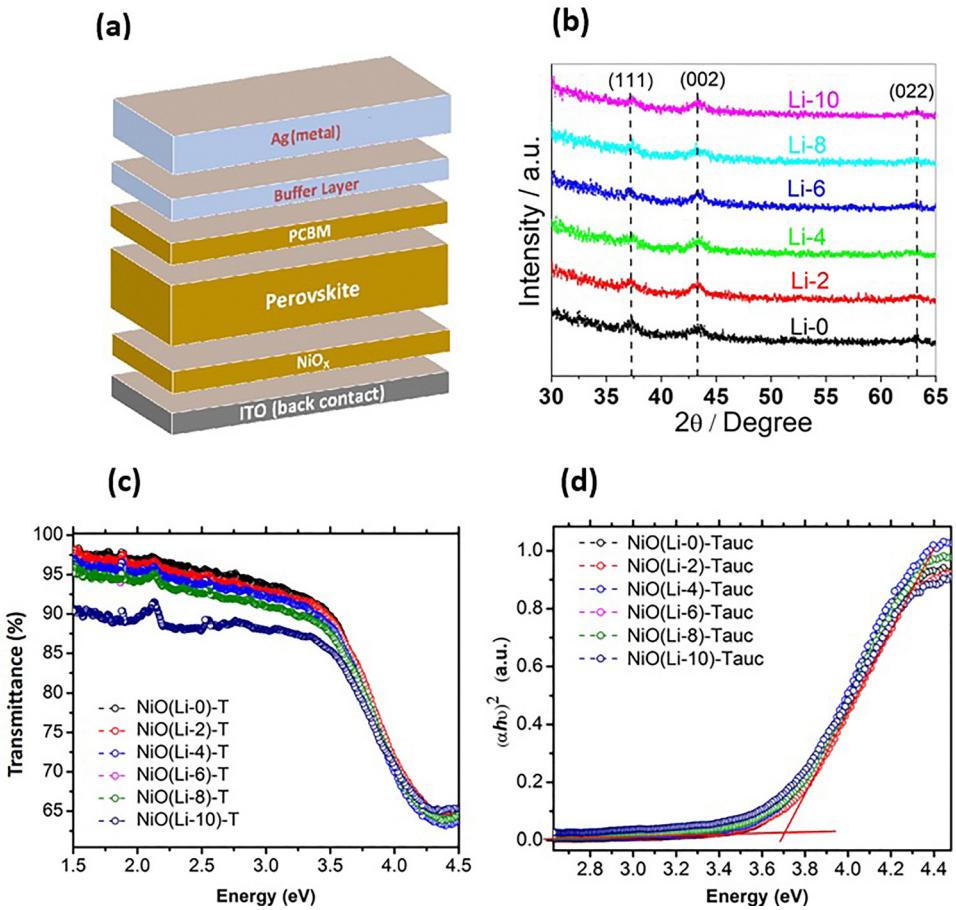

Fig. 1 (a) Device structure of the solar cell, (b) XRD plots of different Li-doped NiO_x films, (c) transmittance of different Li-doped NiO_x films, and (d) Tauc plots for different Li-doped NiO_x films.

Open Access Article. Published on 05 September 2025. Downloaded on 6/8/2026 3:32:19 PM. This article is licensed under a Creative Commons Attribution-NonCommercial 3.0 Unported Licence.

NiO_x shows a nanocrystalline structure, which is confirmed by the top-view scanning electron microscopy (SEM) and atomic force microscopy (AFM) images in Fig. S5 and S6. Fig. 1(b) shows the XRD pattern of undoped and (2–10)% lithium doped NiO_x films. Three distinct peaks at 2θ values of 37.3°, 43.3° and 63.2° correspond to the (111), (002) and (022) planes of cubic phase NiO_x.[28] The analysis also revealed that the incorporation of lithium did not alter the crystal structure of NiO_x. The ionic radii of Li^+ (0.68 Å) and Ni^{2+} (0.69 Å) are similar, which explains the unaltered crystal structure of NiO_x upon lithium doping.[15] The optical transmission of both doped (2–10%) and undoped NiO_x films deposited on glass exhibited high transmittance in the visible spectral range, with an average transmittance exceeding 90% (Fig. 1(c)). As the Li doping concentration increased to 8%, the transmittance of the film slightly decreased; however, at 10% doping, the transmittance decreased significantly. The higher Li content might have induced scattering effects in the NiO_x layer, which caused a reduction in the transmittance.[40] The transmittance of the films was used to determine the bandgap of both Li-doped and undoped NiO_x using the Tauc plot method. The Tauc plot analysis did not show a significant change in optical bandgap (Fig. 1(d)). When the doping concentration increased from 0% to 10%, the bandgap slightly red-shifted from 3.7 eV to 3.67 eV. This result is consistent with a previous study, which reported that on the addition of 5% Li, the bandgap decreased from 3.6 eV (undoped NiO_x) to 3.47 eV.[9] The high transmittance and bandgap of NiO_x remained largely unaffected by Li doping up to a concentration of 8%.

The resistances of the undoped and (2% to 10%) Li-doped NiO_x films were measured using current–voltage (*I–V*) characterization of the respective NiO_x films sandwiched between ITO and high work function gold electrodes. The results revealed a decrease in resistance with an increase in Li-doping up to 4%, after which the resistance remained relatively stable until 8%. A slight increase in resistance was observed at a 10% Li doping level (Fig. S7). This result shows the enhanced electrical conductivity of our NiO_x HTL upon Li doping. X-ray photoelectron spectroscopy (XPS) analysis revealed that the 8% Li doped NiO_x sample exhibited a higher concentration of Ni^{3+} states compared to the undoped sample (Fig. S8). This increase in the Ni^{3+} states contributed to the enhanced p-type behavior of the 8% Li-doped NiO_x layer, thereby improving its electrical conductivity relative to the undoped NiO_x layer.

Study of the perovskite absorber layer

The crystallographic structure of the perovskite layer grown on Li-doped NiO_x with various Li concentrations was studied using grazing incidence X-ray diffraction (GIXRD) analysis and the XRD patterns of the perovskite layer are shown in Fig. 2(a). The results clearly demonstrated the identical diffraction peaks, indicating that the Li doping in the NiO_x layer does not impact the formation of a black-phase perovskite. The major peaks at 14.04°, 19.94°, 24.52°, and 28.3° are, respectively, assigned to the (100), (110), (111), and (200) crystallographic planes of the perovskite.[41] The intensity of the major peaks at the (100) and (200) positions increased with higher Li doping in NiO_x, accompanied by a reduction in their full width at half maximum (FWHM). This enhancement reached its maximum at 8% Li doping, where the peaks exhibited the sharpest profiles. These results indicate the improved crystallinity of the perovskite film on 8% Li-doped NiO_x. To investigate the enhanced crystallinity of the perovskite film deposited on Li-doped NiO_x, we measured the surface roughness of undoped and 8% Li-doped NiO_x films spin-coated on glass substrates using AFM imaging (Fig. 2(b) and (c)). The rms surface roughness of 8% Li-doped NiO_x was 2.92 nm, which was slightly higher compared to that of undoped NiO_x (2.44 nm). The increased roughness might have provided higher nucleation sites for perovskite growth, thereby leading to enhanced crystallinity.[42]

The steady-state photoluminescence (PL) spectra of perovskite films grown on glass, undoped NiO_x and Li-doped NiO_x substrates are presented in Fig. 2(d). The perovskite film grown on Li-doped NiO_x demonstrated a remarkable improvement in the PL characteristics over the perovskite films deposited on glass and undoped NiO_x films. An enhancement in the PL intensity was observed with the addition of Li into NiO_x and it reached the maximum at 8% Li doping in NiO_x. However, a decrease in PL intensity was observed at 10% Li. These results indicate that the presence of Li in NiO_x enhanced the radiative recombination in the perovskite film, most likely through the diffusion of Li-ions into the perovskite and passivation of traps by filling the trap states before photoexcitation. Additionally, a slight redshift in agreement with the transmittance spectra in Fig. 1 was observed as the amount of Li doping increased, which was attributed to the intercalation of Li into the perovskite structure.[43,44]

It is well known that the Li ion is the smallest ion after hydrogen. Li-ions exhibit a high diffusion tendency. The ionic mobility of Li in the perovskite is expected to be higher than that of the intrinsic ions due to its smaller size. The migration of Li through perovskite materials has been demonstrated in $MAPbI_3$ perovskites, which could potentially function as anode materials in Li-ion batteries.[45] Studies have reported that ions from perovskites can move into the hole or electron transport layers, thereby enhancing the carrier-extraction ability and reducing interface recombination, which will result in reduced hysteresis.[36] Also, the migration of Li-ions to the grain boundaries of perovskite crystals has been identified to reduce the nonradiative recombination within the perovskite film.[37] In our case too, the Li-ions migrated from the Li-doped NiO_x HTL into the perovskite, thereby improving the properties of the absorber and offering better carrier generation and extraction.

We studied the depth profile of a 100 nm perovskite layer, deposited on both 4% Li-doped and undoped NiO_x layers using time-of-flight secondary ion mass spectrometry (TOF-SIMS). In the Li-doped sample, we observed clear lithium diffusion towards the perovskite layer, in which a pronounced increase near the perovskite surface exists (Fig. 2(e)). This sharp increase may have resulted either from the accumulation of Li-ions on the perovskite surface due to their smaller size and volatility or from the contamination during the measurement. In contrast,

© 2025 The Author(s). Published by the Royal Society of Chemistry

Open Access Article. Published on 05 September 2025. Downloaded on 6/8/2026 3:32:19 PM.
This article is licensed under a Creative Commons Attribution-NonCommercial 3.0 Unported Licence.

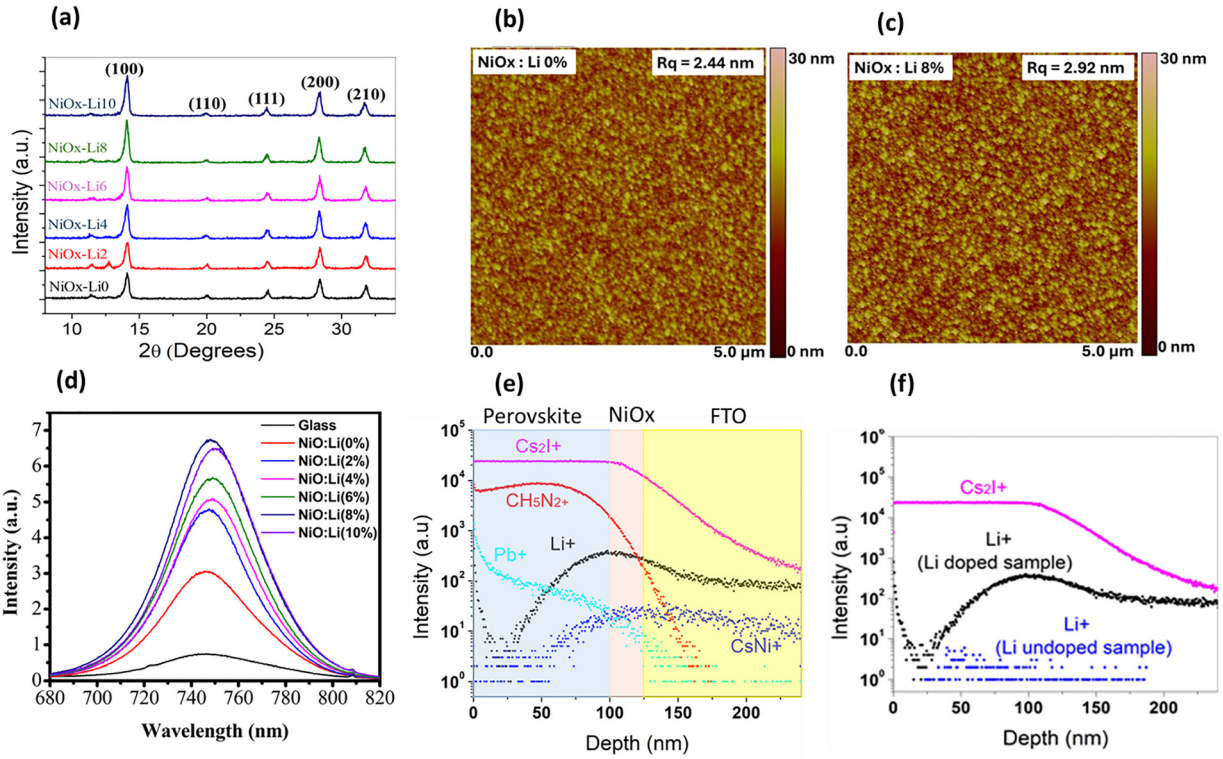

Fig. 2 (a) XRD patterns of perovskite films deposited on different Li-doped NiO_x films, (b) AFM image of Li-0% NiO_x, (c) AFM image of Li-8% NiO_x, (d) steady state PL intensity of perovskite films deposited on different Li-doped NiO_x films, (e) TOF-SIMS depth profile for the device grown on Li-4% NiO_x, and (f) comparison of Li concentrations in the TOF-SIMS profile for devices grown on Li-4% and Li-0% NiO_x films.

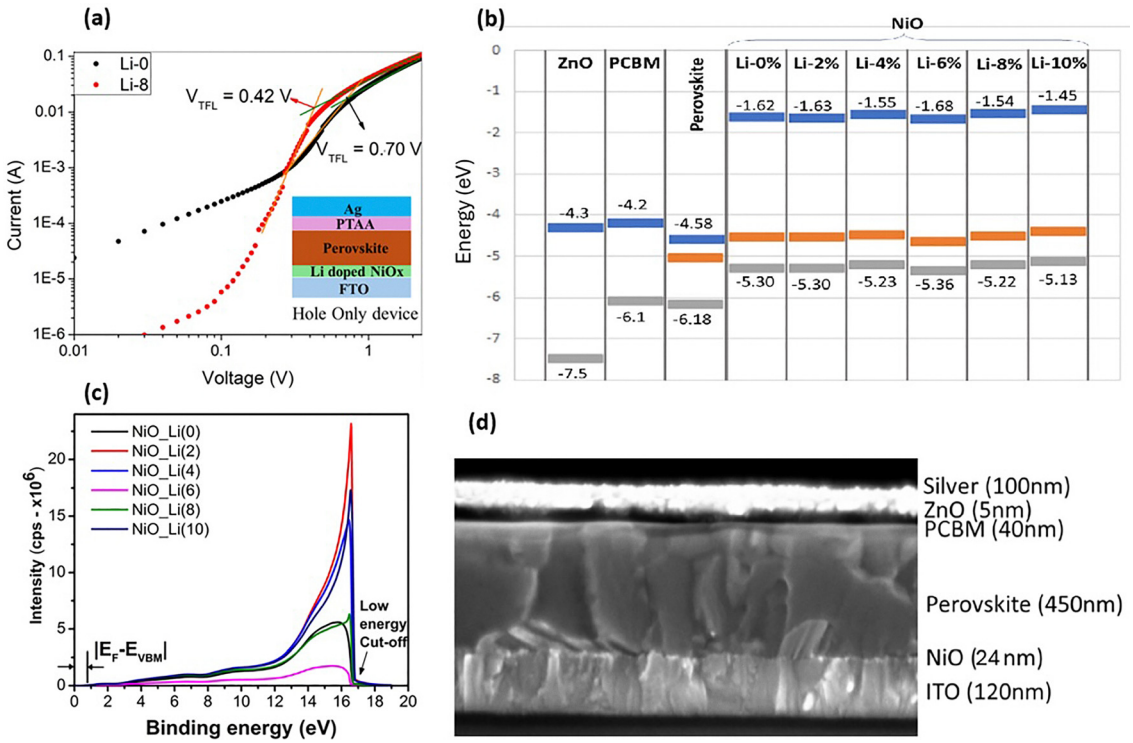

Fig. 3 (a) Dark *JV* curves and V_{TFL} calculation for 0 and 8% Li-doped NiO_x hole only devices (inset: device structure for hole only devices), (b) energy band alignment of perovskites with different Li-doped NiO_x HTLs, (c) UPS characterization of different Li-doped NiO_x HTLs, and (d) cross-sectional SEM image of the perovskite solar cell device.

Open Access Article. Published on 05 September 2025. Downloaded on 6/8/2026 3:32:19 PM.
This article is licensed under a Creative Commons Attribution-NonCommercial 3.0 Unported Licence.

no lithium was detected in the depth profile of the undoped sample (Fig. 2(f) and Fig. S9). Such diffusion of Li-ions from the hole transport layer to the active perovskite layer has indeed been reported.[37]

To further investigate the effect of lithium diffusion into the perovskite layer, we fabricated hole-only devices with the structure of FTO/Li-doped NiO_x/perovskite/PTAA/Ag. These devices were designed to determine the defect density within the bulk perovskite material. Dark *I–V* measurements were carried out to determine the trap-filled-limit voltage (V_{TFL}), which was then used to determine the trap-state density within the perovskite material based on eqn (1), where n_t, ε, q, and L are the trap state density, permittivity of the perovskite, elementary charge (1.6×10^{-19} C) and the thickness of the perovskite layer (450 nm).[46]

$$n_t = \frac{2V_{TFL}\varepsilon}{qL^2} \quad (1)$$

We conducted capacitance measurements of the perovskite layer (Fig. S10) to determine the dielectric constant of the perovskite layer, which was found to be 45. Fig. 3(a) shows a decreased V_{TFL} for the perovskite layer deposited on the 8% Li-doped NiO_x HTL compared to the one deposited on undoped NiO_x, corresponding to trap densities of 1.03×10^{16} cm^{-3} and 1.72×10^{16} cm^{-3}, respectively, which confirms the reduction in trap states after Li doping. The V_{TFL} and n_t calculations for the perovskite layers deposited on all 2 to 10% Li-doped NiO_x are shown in Fig. S11 and Table S1. The results demonstrate a reduction in trap states for the perovskite layers deposited on HTLs with all Li-doping concentrations. These results align with the enhancement in the PL intensity of perovskite films, as discussed earlier.

Ultraviolet photoelectron spectroscopy (UPS) was carried out to obtain energy band information and work function (WF) change of NiO_x films upon Li doping and their alignment with the perovskite energy bands. The band energy values for ZnO and PCBM were taken from the literature and incorporated into the diagram.[9,47] The results of UPS analysis did not reveal significant changes in the energy band position. The optical bandgap for all compositions remained essentially unchanged. The position of the VBM with respect to the Fermi level also remained nearly unchanged, which is consistent with the observed change in resistivity with Li doping. This suggests that the shift in the conduction and valence band positions is attributed mainly to the change in the work function of NiO_x. The work function showed a gradual change, from 4.55 eV to 4.42 eV with a slight difference of 0.13 eV, with increased Li doping (Fig. 3(b)). The work function was determined by calculating the difference between the UV energy and the low energy cut-off as shown in Fig. 3(c). This change might have some impact on the V_{OC} of the devices. However, a direct correlation could not be established.

Performance of the perovskite solar cells

Motivated by the improved crystallinity of perovskite films and passivated nonradiative recombination induced by Li doping, we fabricated inverted planar solar cell devices using PCBM (40 nm) and ZnO (5 nm) as electron transport layers. Our perovskite formulation is a triple cation, CsFAMA (MA: methylammonium, FA: formamidinium and Cs), mixed halide (Cl, Br, and I) perovskite, which is a popular compound that is thermally more stable and enables more reproducible device performance as compared with the highly efficient FAMA perovskite.[48] The cross-sectional SEM image of the complete

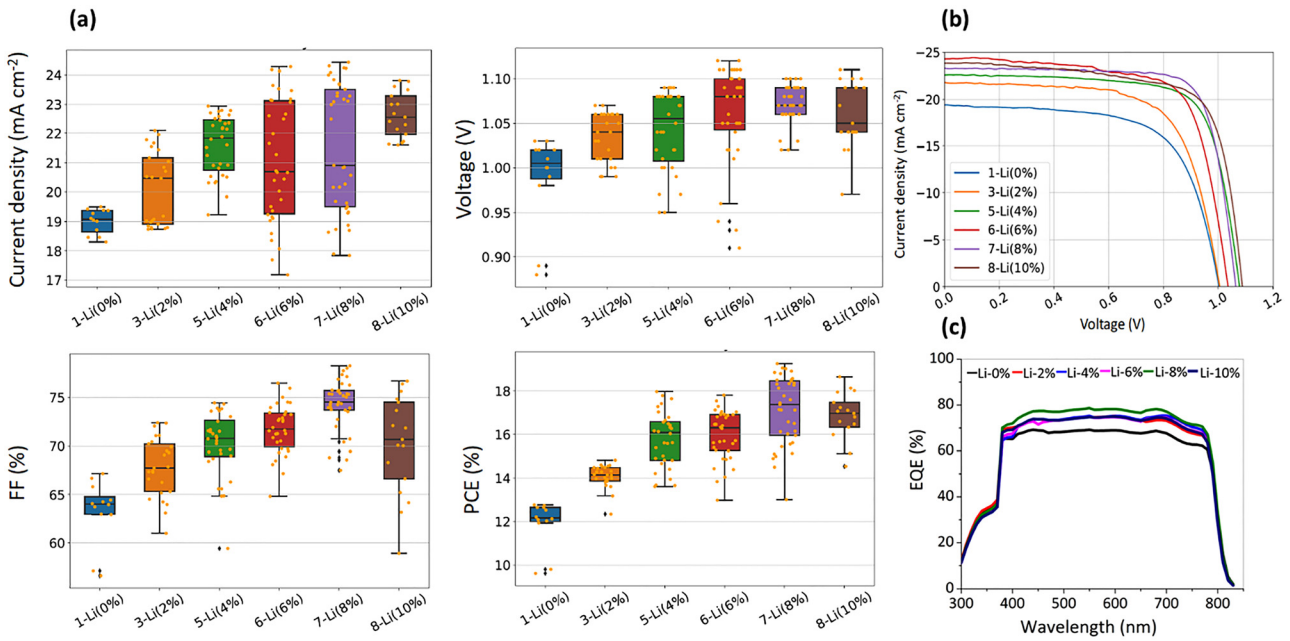

Fig. 4 (a) Device performances of PSCs with different Li doped NiO_x HTLs, (b) *J–V* curves of the best cells for different Li-doped NiO_x devices and (c) EQE plot of perovskite solar cells on different Li-doped NiO_x HTLs.

© 2025 The Author(s). Published by the Royal Society of Chemistry

Open Access Article. Published on 05 September 2025. Downloaded on 6/8/2026 3:32:19 PM. This article is licensed under a Creative Commons Attribution-NonCommercial 3.0 Unported Licence.

Table 1 Performance of different Li doped NiO_x based perovskite solar cells

Sample	J_{sc} (mA cm^{-2})	V_{OC} (V)	Fill factor (%)	Efficiency (%)
Li-0%	19.00 ± 0.37	0.99 ± 0.05	63.35 ± 3.02	11.47 ± 1.30
Li-2%	20.17 ± 1.22	1.03 ± 0.03	67.83 ± 3.08	14.10 ± 0.52
Li-4%	21.54 ± 1.04	1.04 ± 0.04	70.01 ± 3.34	15.79 ± 1.26
Li-6%	21.05 ± 2.08	1.06 ± 0.06	71.74 ± 2.51	15.98 ± 1.16
Li-8%	21.44 ± 2.17	1.07 ± 0.02	74.18 ± 2.62	17.00 ± 1.57
Li-10%	22.61 ± 1.06	1.06 ± 0.03	70.45 ± 5.00	16.70 ± 1.05

device is shown in Fig. 3(d), which shows a compact perovskite layer along with the other layers.

The device performances were compared using a box and whisker plot, which showed an improvement in all the solar cell parameters with increased Li doping (Fig. 4(a)). The overall device performance with Li doping in the NiO_x HTL is summarized in Table 1 and the best *JV* curves are shown in Fig. 4(b). The increase in the average current density of solar cell devices upon Li doping in NiO_x can be attributed to the improved radiative recombination of the charge carriers in the absorber layer, resulting in higher carrier collection, which led to a boost in the current density. This is further proved by the external quantum efficiency (EQE) plots of the PSC devices based on different lithium doped NiO_x films (Fig. 4(c)), which indicate the improved perovskite absorber quality upon doping NiO_x with lithium.

Likewise, the enhancement in the open circuit voltage (V_{OC}) could be attributed to the proper energy level alignment of the perovskite valence band with the valence band of Li-doped NiO_x, resulting in smaller energy offsets. The reduced number of defect sites in the perovskites along with a decrease in the series resistance offered by Li-doped NiO_x resulted in improvements in both the V_{OC} as well as the fill factor (FF) of the solar cell devices. These improvements in all the parameters achieved by doping up to 8% Li concentration in NiO_x contributed to the enhanced PCE of the devices. With these aggregate effects, the PCE of the best device increased from approximately 12% without Li doping to a maximum of 19.3% at 8% Li doping, representing a 60.8% improvement.

Conclusions

This research investigated the effect of Li doping on the electrical and optical properties of the NiO_x hole transport layer. Li doping in NiO_x improved the crystallinity and optical properties of the subsequent perovskite absorber layer, as confirmed by the results. Furthermore, TOF-SIMS analysis of the perovskite film deposited on lithium doped NiO_x revealed the migration of small Li-ions from the Li-doped NiO_x HTL into the perovskite layer. This migration enhanced the device performance by passivating the nonradiative recombination centers and improving the crystallinity of the perovskite material. As a result of these combined effects, the PCE of the best device increased by 60.8%, increasing from approximately 12% without Li doping to a peak of 19.3% with 8% Li doping.

Author contributions

Rajbhandari performed the experiment, analyzed the data and wrote the manuscript. Rijal and Chen performed further analysis and edited the manuscript. Choudhary and Efstathiadis performed the TOF-SIMS measurement and the analysis of the depth-profile data. Dhakal conceptualized the idea, secured funding, advised the research, and edited the manuscript.

Conflicts of interest

There are no conflicts to declare.

Data availability

The data generated in this research are available in the Mendeley data repository at DOI: **10.17632/t82zfxrhwf.1**.

Supplementary information is available. See DOI: **https://doi.org/10.1039/d5ya00072f**.

Acknowledgements

This work was supported in part by the National Science Foundation under grant number 1751946.

References

1 S. Liu, V. P. Biju, Y. Qi, W. Chen and Z. Liu, Recent Progress in the Development of High-Efficiency Inverted Perovskite Solar Cells, *NPG Asia Mater.*, 2023, **15**(1), 1–28, DOI: **10.1038/s41427-023-00474-z**.

2 Z. Chen, W. Reyes Ramos, G. Singh Khinda, J. Amey, M. D. Poliks, D. M. Smilgies and T. P. Dhakal, Multipass Inkjet Printing of Lead Halide Perovskite Pixels onto Flexible Substrates, *ACS Appl. Opt. Mater.*, 2023, **1**(9), 1527–1534, DOI: **10.1021/ACSAOM.3C00164**.

3 Z. Chen and T. P. Dhakal, Room Temperature Synthesis of Lead-Free $FASnI_3$ perovskite Nanocrystals with Improved Stability by SnF_2 additive, *Appl. Phys. Rev.*, 2023, **10**(1), 011404, DOI: **10.1063/5.0125100**.

4 L. Meng, J. You, T.-F. Guo and Y. Yang, Recent Advances in the Inverted Planar Structure of Perovskite Solar Cells, *Acc. Chem. Res.*, 2016, **49**(1), 155–165, DOI: **10.1021/acs.accounts.5b00404**.

5 D. Luo, W. Yang, Z. Wang, A. Sadhanala, Q. Hu, R. Su, R. Shivanna, G. F. Trindade, J. F. Watts, Z. Xu, T. Liu, K. Chen, F. Ye, P. Wu, L. Zhao, J. Wu, Y. Tu, Y. Zhang, X. Yang, W. Zhang, R. H. Friend, Q. Gong, H. J. Snaith and R. Zhu, Enhanced Photovoltage for Inverted Planar Heterojunction Perovskite Solar Cells, *Science*, 2018, **360**(6396), 1442–1446.

6 L. Zhao, X. Sun, Q. Yao, S. Huang, L. Zhu, J. Song, Y. Zhao and Y. Qiang, Field-Effect Control in Hole Transport Layer Composed of Li:NiO/NiO for Highly Efficient Inverted Planar Perovskite Solar Cells, *Adv. Mater. Interfaces*, 2022, **9**(2), 2101562, DOI: **10.1002/ADMI.202101562**.

© 2025 The Author(s). Published by the Royal Society of Chemistry

Open Access Article. Published on 05 September 2025. Downloaded on 6/8/2026 3:32:19 PM. This article is licensed under a Creative Commons Attribution-NonCommercial 3.0 Unported Licence.

7 Z. Qiu, H. Gong, G. Zheng, S. Yuan, H. Zhang, X. Zhu, H. Zhou and B. Cao, Enhanced Physical Properties of Pulsed Laser Deposited NiO Films *via* Annealing and Lithium Doping for Improving Perovskite Solar Cell Efficiency, *J. Mater. Chem. C*, 2017, **5**(28), 7084–7094, DOI: **10.1039/C7TC01224A**.

8 K. Zhao, Y. Zhao, Y. Tan, K. Hu and Z.-S. Wang, Boosting the Conductivity of the NiO_x Layer through Cerium Doping for Efficient Planar Inverted Perovskite Solar Cells, *ACS Appl. Energy Mater.*, 2021, acsaem.1c01330, DOI: **10.1021/ACSAEM.1C01330**.

9 W. Chen, Y. Wu, Y. Yue, J. Liu, W. Zhang, X. Yang, H. Chen, E. Bi, I. Ashraful, M. Grätzel and L. Han, Efficient and Stable Large-Area Perovskite Solar Cells with Inorganic Charge Extraction Layers, *Science*, 2015, **350**(6263), 944–948, DOI: **10.1126/SCIENCE.AAD1015**.

10 A. Bashir, L. J. Haur, S. Shukla, D. Gupta, T. Baikie, S. Chakraborty, R. Patidar, A. Bruno, S. Mhaisalkar and Z. Akhter, Cu-Doped Nickel Oxide Interface Layer with Nanoscale Thickness for Efficient and Highly Stable Printable Carbon-Based Perovskite Solar Cell, *Sol. Energy*, 2019, **182**, 225–236, DOI: **10.1016/j.solener.2019.02.056**.

11 K. C. Hsiao, B. T. Lee, M. H. Jao, T. H. Lin, C. H. Hou, J. J. Shyue, M. C. Wu and W. F. Su, Chloride Gradient Render Carrier Extraction of Hole Transport Layer for High V_{OC} and Efficient Inverted Organometal Halide Perovskite Solar Cell, *Chem. Eng. J.*, 2021, **409**, 128100, DOI: **10.1016/J.CEJ.2020.128100**.

12 A. C. Nkele, A. C. Nwanya, N. M. Shinde, S. Ezugwu, M. Maaza, J. S. Shaikh and F. I. Ezema, The Use of Nickel Oxide as a Hole Transport Material in Perovskite Solar Cell Configuration: Achieving a High Performance and Stable Device, *Int. J. Energy Res.*, 2020, **44**(13), 9839–9863, DOI: **10.1002/ER.5563**.

13 A. Yi, S. Chae, H. Lee, S. H. Lee, D. Kim and H. J. Kim, Synergistic Effect of Codoped Nickel Oxide Hole–Transporting Layers for Highly Efficient Inverted Perovskite Solar Cells, *Sol. RRL*, 2021, **5**(9), 2100243, DOI: **10.1002/SOLR.202100243**.

14 J. J. Zhao, X. Su, Z. Mi, Y. Zhang, Y. J. Hu, H. J. Guo, Y. N. Jiao, Y. X. Zhang, Y. Shi, W. Z. Hao, J. W. Wu, Y. Wang, C. F. Gao and G. Z. Cao, Trivalent Ni Oxidation Controlled through Regulating Lithium Content to Minimize Perovskite Interfacial Recombination, *Rare Met.*, 2022, **41**(1), 96–105, DOI: **10.1007/S12598-021-01800-6/FIGURES/6**.

15 Z. Saki, K. Sveinbjörnsson, G. Boschloo and N. Taghavinia, The Effect of Lithium Doping in Solution-Processed Nickel Oxide Films for Perovskite Solar Cells, *ChemPhysChem*, 2019, **20**(24), 3322–3327, DOI: **10.1002/CPHC.201900856**.

16 S. Lany, J. Osorio-Guillén and A. Zunger, Origins of the Doping Asymmetry in Oxides: Hole Doping in NiO *versus* Electron Doping in ZnO, *Phys. Rev. B: Condens. Matter Mater. Phys.*, 2007, **75**, 241203(R), DOI: **10.1103/PhysRevB.75.241203**.

17 W. Chen, F.-Z. Liu, X.-Y. Feng, A. B. Djurišić, W. K. Chan and Z.-B. He, Cesium Doped NiO_x as an Efficient Hole Extraction Layer for Inverted Planar Perovskite Solar Cells, *Adv. Energy Mater.*, 2017, **7**(19), 1700722, DOI: **10.1002/AENM.201700722**.

18 S. Teo, Z. Guo, Z. Xu, C. Zhang, Y. Kamata, S. Hayase and T. Ma, The Role of Lanthanum in a Nickel Oxide-Based Inverted Perovskite Solar Cell for Efficiency and Stability Improvement, *ChemSusChem*, 2019, **12**(2), 518–526, DOI: **10.1002/CSSC.201802231**.

19 L. Zhao, G. Su, W. Liu, L. Cao, J. Wang, Z. Dong and M. Song, Optical and Electrochemical Properties of Cu-Doped NiO Films Prepared by Electrochemical Deposition, *Appl. Surf. Sci.*, 2011, **257**(9), 3974–3979, DOI: **10.1016/J.APSUSC.2010.11.160**.

20 X. Wan, Y. Jiang, Z. Qiu, H. Zhang, X. Zhu, I. Sikandar, X. Liu, X. Chen and B. Cao, Zinc as a New Dopant for NiO_x-Based Planar Perovskite Solar Cells with Stable Efficiency near 20%, *ACS Appl. Energy Mater.*, 2018, **1**(8), 3947–3954, DOI: **10.1021/ACSAEM.8B00671/ASSET/IMAGES/LARGE/AE-2018-00671W_0008.JPEG**.

21 B. Parida, S. Yoon, J. Ryu, S. Hayase, S. M. Jeong and D.-W. Kang, Boosting the Conversion Efficiency Over 20% in MAPbI 3 Perovskite Planar Solar Cells by Employing a Solution-Processed Aluminum-Doped Nickel Oxide Hole Collector, *ACS Appl. Mater. Interfaces*, 2020, 12, DOI: **10.1021/acsami.0c04618**.

22 Y. Xie, K. Lu, J. Duan, Y. Jiang, L. Hu, T. Liu, Y. Zhou and B. Hu, Enhancing Photovoltaic Performance of Inverted Planar Perovskite Solar Cells by Cobalt-Doped Nickel Oxide Hole Transport Layer, *ACS Appl. Mater. Interfaces*, 2018, **10**(16), 14153–14159, DOI: **10.1021/ACSAMI.8B01683**.

23 U. K. Thakur, P. Kumar, S. Gusarov, A. E. Kobryn, S. Riddell, A. Goswami, K. M. Alam, S. Savela, P. Kar, T. Thundat, A. Meldrum and K. Shankar, Consistently High V_{OC} Values in p–i–n Type Perovskite Solar Cells Using Ni^{3+}-Doped NiO Nanomesh as the Hole Transporting Layer, *ACS Appl. Mater. Interfaces*, 2020, **12**(10), 11467–11478, DOI: **10.1021/ACSAMI.9B18197**.

24 W. Chen, Y. Zhou, L. Wang, Y. Wu, B. Tu, B. Yu, F. Liu, H.-W. Tam, G. Wang, A. B. Djurišić, L. Huang and Z. He, Molecule-Doped Nickel Oxide: Verified Charge Transfer and Planar Inverted Mixed Cation Perovskite Solar Cell, *Adv. Mater.*, 2018, **30**(20), 1800515, DOI: **10.1002/ADMA.201800515**.

25 Y. Wu, F. Xie, H. Chen, X. Yang, H. Su, M. Cai, Z. Zhou, T. Noda and L. Han, Thermally Stable $MAPbI_3$ Perovskite Solar Cells with Efficiency of 19.19% and Area over 1 cm^2 Achieved by Additive Engineering, *Adv. Mater.*, 2017, **29**(28), 1701073, DOI: **10.1002/ADMA.201701073**.

26 F. P. Gokdemir Choi, H. Moeini Alishah and S. Gunes, Cerium and Zinc Co-Doped Nickel Oxide Hole Transport Layers for Gamma-Butyrolactone Based Ambient Air Fabrication of $CH_3NH_3PbI_3$ Perovskite Solar Cells, *Appl. Surf. Sci.*, 2021, **563**, 150249, DOI: **10.1016/j.apsusc.2021.150249**.

27 I. Sta, M. Jlassi, M. Hajji and H. Ezzaouia, Structural, Optical and Electrical Properties of Undoped and Li-Doped NiO Thin Films Prepared by Sol–Gel Spin Coating Method, *Thin Solid Films*, 2014, **555**, 131–137, DOI: **10.1016/j.tsf.2013.10.137**.

 © 2025 The Author(s). Published by the Royal Society of Chemistry

Open Access Article. Published on 05 September 2025. Downloaded on 6/8/2026 3:32:19 PM. This article is licensed under a Creative Commons Attribution-NonCommercial 3.0 Unported Licence.

28 D. P. Joseph, M. Saravanan, B. Muthuraaman, P. Renugambal, S. Sambasivam, S. P. Raja, P. Maruthamuthu and C. Venkateswaran, Spray Deposition and Characterization of Nanostructured Li Doped NiO Thin Films for Application in Dye-Sensitized Solar Cells, *Nanotechnology*, 2008, **19**, 485707, DOI: 10.1088/0957-4484/19/48/485707.

29 J. H. Park, J. Seo, S. Park, S. S. Shin, Y. C. Kim, N. J. Jeon, H. W. Shin, T. K. Ahn, J. H. Noh, S. C. Yoon, C. S. Hwang and S. I. L. Seok, Efficient $CH_3NH_3PbI_3$ Perovskite Solar Cells Employing Nanostructured p-Type NiO Electrode Formed by a Pulsed Laser Deposition, *Adv. Mater.*, 2015, **27**(27), 4013–4019, DOI: 10.1002/adma.201500523.

30 W.-L. Jang, Y.-M. Lu, W.-S. Hwang and W.-C. Chen, Electrical Properties of Li-Doped NiO Films, *J. Eur. Ceram. Soc.*, 2010, **30**, 503–508, DOI: 10.1016/j.jeurceramsoc.2009.05.041.

31 S. Oswald and W. Brückner, XPS Depth Profile Analysis of Non-Stoichiometric NiO Films, *Surf. Interface Anal.*, 2004, **36**(1), 17–22, DOI: 10.1002/sia.1640.

32 D. Di Girolamo, A. B. Francesco Di Giacomo, F. Matteocci, A. Giacomo Marrani and D. Dini, Progress, Highlights and Perspectives on NiO in Perovskite Photovoltaics, *Chem. Sci.*, 2020, **11**, 7746–7759, DOI: 10.1039/d0sc02859b.

33 P. S. Patil and L. D. Kadam, Preparation and Characterization of Spray Pyrolyzed Nickel Oxide (NiO) Thin Films, *Appl. Surf. Sci.*, 2002, **199**(1–4), 211–221, DOI: 10.1016/S0169-4332(02)00839-5.

34 T. Dutta, P. Gupta, A. Gupta and J. Narayan, Effect of Li Doping in NiO Thin Films on Its Transparent and Conducting Properties and Its Application in Heteroepitaxial p–n Junctions, *J. Appl. Phys.*, 2010, **108**(8), 083715, DOI: 10.1063/1.3499276.

35 W. Nie, H. Tsai, J.-C. Blancon, F. Liu, C. C. Stoumpos, B. Traore, M. Kepenekian, O. Durand, C. Katan, S. Tretiak, J. Crochet, P. M. Ajayan, M. G. Kanatzidis, J. Even and A. D. Mohite, Critical Role of Interface and Crystallinity on the Performance and Photostability of Perovskite Solar Cell on Nickel Oxide, *Adv. Mater.*, 2018, **30**(5), 1703879, DOI: 10.1002/ADMA.201703879.

36 Z. Li, C. Xiao, Y. Yang, S. P. Harvey, D. H. Kim, J. A. Christians, M. Yang, P. Schulz, S. U. Nanayakkara, C. S. Jiang, J. M. Luther, J. J. Berry, M. C. Beard, M. M. Al-Jassim and K. Zhu, Extrinsic Ion Migration in Perovskite Solar Cells, *Energy Environ. Sci.*, 2017, **10**(5), 1234–1242, DOI: 10.1039/c7ee00358g.

37 C. Xiao, F. Zhang, Z. Li, S. P. Harvey, X. Chen, K. Wang, C. S. Jiang, K. Zhu and M. Al-Jassim, Inhomogeneous Doping of Perovskite Materials by Dopants from Hole-Transport Layer, *Matter*, 2020, **2**(1), 261–272, DOI: 10.1016/j.matt.2019.10.005.

38 P. P. Rajbhandari and T. P. Dhakal, Limit of Incorporating Cesium Cations into Formamidinium–Methylammonium Based Mixed Halide Perovskite Solar Cells, *Nanotechnology*, 2020, **31**(13), 135406, DOI: 10.1088/1361-6528/AB6230.

39 P. P. Rajbhandari and T. P. Dhakal, Low Temperature ALD Growth Optimization of ZnO, TiO_2, and Al_2O_3 to Be Used as a Buffer Layer in Perovskite Solar Cells, *J. Vac. Sci. Technol., A*, 2020, **38**(3), 032406, DOI: 10.1116/1.5139247.

40 K. H. Kim, C. Takahashi, Y. Abe and M. Kawamura, Effects of Cu Doping on Nickel Oxide Thin Film Prepared by Sol–Gel Solution Process, *Optik*, 2014, **125**(12), 2899–2901, DOI: 10.1016/J.IJLEO.2013.11.074.

41 G. Zheng, C. Zhu, J. Ma, X. Zhang, G. Tang, R. Li, Y. Chen, L. Li, J. Hu, J. Hong, Q. Chen, X. Gao and H. Zhou, Manipulation of Facet Orientation in Hybrid Perovskite Polycrystalline Films by Cation Cascade, *Nat. Commun.*, 2018, **9**(1), 1–11, DOI: 10.1038/s41467-018-05076-w.

42 P. Grosfils and J. F. Lutsko, Impact of Surface Roughness on Crystal Nucleation, *Crystals*, 2021, **11**(1), 4, DOI: 10.3390/CRYST11010004.

43 Z. Fang, H. He, L. Gan, J. Li and Z. Ye, Understanding the Role of Lithium Doping in Reducing Nonradiative Loss in Lead Halide Perovskites, *Adv. Sci.*, 2018, **5**(12), 1–6, DOI: 10.1002/advs.201800736.

44 A. Xie, C. Hettiarachchi, F. Maddalena, M. E. Witkowski, M. Makowski, W. Drozdowski, A. Arramel, A. T. S. Wee, S. V. Springham, P. Q. Vuong, H. J. Kim, C. Dujardin, P. Coquet, M. D. Birowosuto and C. Dang, Lithium-Doped Two-Dimensional Perovskite Scintillator for Wide-Range Radiation Detection, *Commun. Mater.*, 2020, **1**(1), 1–10, DOI: 10.1038/s43246-020-0038-x.

45 H.-R. Xia, W. T. Sun and L.-M. Peng, Hydrothermal synthesis of organometal halide perovskites for Li-ion batteries, *Chem. Commun.*, 2015, **51**, 13787–13790.

46 V. M. Le Corre, E. A. Duijnstee, O. El Tambouli, J. M. Ball, H. J. Snaith, J. Lim and L. J. A. Koster, Revealing Charge Carrier Mobility and Defect Densities in Metal Halide Perovskites *via* Space-Charge-Limited Current Measurements, *ACS Energy Lett.*, 2021, **6**(3), 1087–1094, DOI: 10.1021/ACSENERGYLETT.0C02599/ASSET/IMAGES/MEDIUM/NZ0C02599_M005.GIF.

47 S. Chatterjee and A. J. Pal, Introducing Cu_2O Thin Films as a Hole-Transport Layer in Efficient Planar Perovskite Solar Cell Structures, *J. Phys. Chem. C*, 2016, **120**(3), 1428–1437, DOI: 10.1021/acs.jpcc.5b11540.

48 M. Saliba, T. Matsui, J. Y. Seo, K. Domanski, J. P. Correa-Baena, M. K. Nazeeruddin, S. M. Zakeeruddin, W. Tress, A. Abate, A. Hagfeldt and M. Grätzel, Cesium-Containing Triple Cation Perovskite Solar Cells: Improved Stability, Reproducibility and High Efficiency, *Energy Environ. Sci.*, 2016, **9**(6), 1989–1997, DOI: 10.1039/C5EE03874J.